Article

On the Enhancement of Energy Storage Performance in Modified Relaxor Ferroelectric Ceramics for Pulsed Power Applications

Hao Zhang [1,2], Zhe Zhu [1], Zhonghua Yao [1,2,*], Hua Hao [1,2], Lingyun Wang [3,*], Minghe Cao [1] and Hanxing Liu [1,2]

1   School of Material Science and Engineering, Wuhan University of Technology, Wuhan 430070, China
2   Sanya Science and Education Innovation Park, Wuhan University of Technology, Sanya 572000, China
3   Institute of Fluid Physics, CAEP, Mianyang 621900, China
*   Correspondence: yaozhhua@whut.edu.cn (Z.Y.); 101kpa@sina.com (L.W.)

Abstract: Relaxor-type ferroelectrics show important potential in energy storage fields due to their significantly enhanced energy performance and good temperature stability compared to normal ferroelectrics. Here, a novel, high-performance ternary composition, $(0.4-x)BiFeO_3$-$xBi(Mg_{1/2}Ti_{1/2})O_3$–$0.6BaTiO_3$ (x = 0.2, 0.25, 0.3, 0.35, 0.4), was designed by compositional modulation, which displays typical relaxor characteristics. The optimum energy storage properties can be attained at x = 0.35, accompanied by energy efficiency of 84.87%, a promising energy storage density of 2.3 J/cm^3 and good temperature stability of less than 10% over 20–160 °C. Moreover, the samples provide stable cycling fatigue after 10^5 cycles and a fast discharge time of $t_{0.9} < 0.1$ μs, indicative of promising applications in energy units.

Keywords: ceramics; perovskites; dielectrics; energy storage; lead-free ceramics

1. Introduction

In recent years, the increasing sustainability problems have forced societies to develop and utilize renewable and environmentally friendly energy sources [1–3]. As a large amount of new energy needs to be stored in the form of electric energy, the storage technology of electric energy has been paid much attention. At present, electrical energy storage mostly depends on the following methods: electrochemical supercapacitors, batteries and dielectric capacitors [4,5]. Typically, batteries have a high energy storage density; however, because they involve chemical reactions and have a slow charge and discharge rate, their power density is low. However, dielectric capacitors have typical characteristics of high power density, ultrafast charge and discharge rates, long lifetimes and so on, and because the charge and discharge process does not involve an electrochemical reaction, they are safer and more reliable than the other two. For electrochemical supercapacitors, the power density and energy storage density are moderate. In pulsed power systems, dielectric capacitors have been widely studied and applied because of their excellent characteristics. To maximize the energy density of capacitors, dielectrics often need to have high dielectric polarization as well as dielectric breakdown strength (BDS), and, more importantly, the question of how to coordinate the relationship between the two has become a new topic. Currently, commercially available dielectrics for high-power applications consist primarily of polymers or ceramics that typically possess a limited energy density of <2 J/cm^3 [6–14].

Many attempts have been made to improve the energy storage performance (ESPf) of dielectrics. It is generally believed that, for normal ferroelectrics, the hysteresis loop exhibits a saturated tetragonal shape and large polarization intensity. The ferroelectric domain loses a great deal of energy during the reversal process, resulting in low energy efficiency. For relaxor ferroelectrics, there is a thin hysteresis loop and they usually exhibit low remnant polarization, which is beneficial to obtain enhanced energy properties. Many compositions

have been developed, especially in lead-free systems, such as BNT and BFO, and NN-based systems, by introducing heterovalent ions to construct relaxation phases [15–18]. Specifically, BiFeO$_3$-BaTiO$_3$ (BF-BT) solid solutions have received considerable attention as promising candidates in the field of ceramic dielectric-based energy storage materials. It has been established that BiFeO$_3$-BaTiO$_3$ has a high Curie temperature and a significant amount of polarization ($P_{max} > 40$ μC/cm^2) at the structural phase boundary [19–21]. It has been reported that the formation of locally, weakly coupled polar nano-regions (PNRs) in ferroelectrics can induce relaxor characteristics, accompanied by ferroelectric domain modulation. In the BiFeO$_3$-containing system, stripe-like polar nano-domain PNRs (only 3 nm) were obtained due to relaxor characteristics [19]. This structure permits the polarization response to be almost linear, without hysteresis, thus effectively improving the ESPf of these materials. Similarly, the introduction of ions (Ba^{2+}, Zn^{2+}, Ta^{5+}) tailored with different chemical valences and radii leads to the local compositional disorder of BF-BT-based ferroelectric ceramics in terms of the enhancement of its relaxor behavior, resulting in high energy storage density (W) [16]. However, the limited energy performance for BF-containing compositions can be ascribed to leakage at high fields. In view of this, many methods have been carried out to optimize it. Many materials have been selected as modifiers to tailor the ESPf of BF-BT ceramics, such as LMT, BMN, Nb, and so on [22–24]. By incorporating La$_2$O$_3$ and MnO$_2$, Zhu et al. discovered a significant increase in the BDS of 0.52BF-0.48BT ceramics. La-modified 0.52BF-0.48BT ceramics exhibited an increased W_{rec} of 1.22 J/cm^3 with η = 58% under ~140 kV/cm compared with the undoped ones due to the increased FE phases, decreased grain size, and facilitated densification. These can lead to enhanced ΔP ($P_{max} - P_r$) as well as BDS [25]. Wang et al. reported that in 0.75BiFeO$_3$–0.25BaTiO$_3$ ceramics, Nd substitution can significantly elevate energy storage, with 15mol% Nd content, accompanied by a promising W of 4.1 J/cm^3 but an ultralow η of 41.3% under 180 kV/cm [26]. Moreover, Sm substitution can significantly impact the grain size and the density of BF-BT ceramics, facilitating the enhancement of the BDS [27].

As reported, the introduction of BiFeO$_3$ can obviously increase the energy storage density of dielectric materials, especially for dielectric thin films. In this case, the authors wished to make use of the high polarization of BiFeO$_3$ to partly replace BMT to improve the energy storage performance of BMT-BT compositions. Here, a composition of (0.4−x)BiFeO$_3$-xBi(Mg$_{1/2}$Ti$_{1/2}$)O$_3$–0.6BaTiO$_3$ ceramic was selected as the base material to develop new energy storage materials with from large polarization and an elevated BDS.

2. Experimental

A series of (0.4−x)BiFeO$_3$-xBi(Mg$_{1/2}$Ti$_{1/2}$)O$_3$–0.6BaTiO$_3$ ((0.4−x)BF-xBMT-0.6BT, x = 0.2, 0.25, 0.3, 0.35, 0.4) ceramics were prepared by stoichiometry. The original components included Bi$_2$O$_3$ (≥99.0%), MgO (≥99.0%), TiO$_2$ (≥98.0%), Fe$_2$O$_3$ (≥99.0%), and BaCO$_3$ (≥99.0%). All the raw materials used here were produced by Sinopharm Chemical Reagent Co. Ltd. The powders were milled with absolute ethyl alcohol for 24 h with a zirconia ball. The horizontal ball mill (GMS3–4) had a speed of 120 r/min. The size and mass ratio of the zirconia ball used were M(3 mm):M(5 mm):M(7 mm)= 3:4:3. The calcination was carried out for the powders at 800 °C for 2 h after drying and then they were granulated with a PVA binder. Ceramic discs of diameter ~12 mm and thickness ~1.0 mm were pressed under 150 MPa. The samples were calcined at 600 °C for 2 h to burn out the PVA, and then sintered at 1120 °C for 2h. For sintering, they were heated at 2 °C/min and then cooled in a furnace. Raw material powders were used to cover ceramic chips to prevent Bi volatilization. Lastly, ceramics were ground and polished to ~0.2 mm in thickness and coated with Ag electrodes with a diameter of nearly 3 mm.

A PANalytical-type X-ray diffraction (XRD, X'Pert PRO) with Cu K_α radiation was employed to describe the phase structure of the ceramics. SEM (Quanta 450FEG, FEI Company) was used to observe the microstructures and grain orientation. Prior to the investigation, the samples were covered with a thin, conductive platinum layer deposited by the ion sputtering method. An LCR analyzer (E4980A, Agilent, Palo Alto, CA, USA)

was introduced to measure the dielectric temperature dependence in a temperature range of 25 to 350 °C, with a test frequency of 1 kHz, 10 kHz, 100 kHz, 1 MHz, respectively. The dielectric breakdown strength and ESPf were measured using a 0.15-mm-thick ceramic disc. A ferroelectric testing system (PKCPE1701, PolyK Technologies, Philipsburg, PA, USA) was employed to measure the energy storage properties, P-E loops, dielectric breakdown strength, temperature stability, and fatigue performance. Charging and discharging characteristics were measured with an RC circuit with a load resistance of 1000 Ω, using a ferroelectric analyzer.

3. Results and Discussion

XRD patterns for the (0.4−x)BF-xBMT-0.6BT ceramics are shown in Figure 1a. All samples have a typical perovskite diffraction peak without impurity, indicative of the formation of a complete solid solution. Splitting of the (110) peak cannot be observed in Figure 1b, indicative of the pseudo-cubic phase. The absence of a shift in the diffraction peak can be ascribed to the small difference in lattice due to the similar average ionic radii ($Fe^{3+} \sim 0.64$ Å, $(Mg_{1/2}Ti_{1/2})^{3+} \sim 0.662$Å) [28,29].

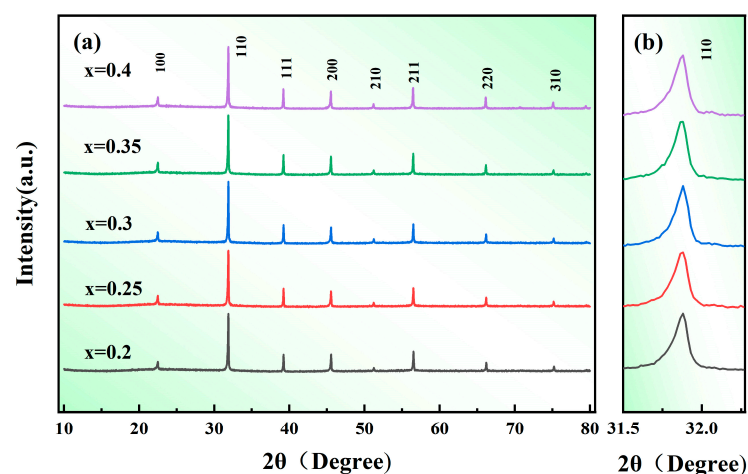**Figure 1.** (**a**) XRD spectra (0.4−x)BF-xBMT-0.6BT ceramics; (**b**) locally magnified (110) diffraction peaks.

Figure 2 shows the fractured-surface SEM images of the (0.4−x)BF-xBMT-0.6BT ceramics. The density of the ceramic samples was measured via the Archimedes drainage method and the relative density was calculated. The relative density of the ceramic samples was greater than 90%. It could be found that all ceramics showed uniform and dense microstructures. The grain size distributions were measured to obtain the average grain size. It is clear that the average grain size becomes small from 6.97 μm at x = 0.2 to 1.36 μm at x = 0.4 with increasing BMT, respectively. The decrease in grain size may be due to defects caused by doping with ions of different valence states [30]. With the increasing BMT, the concentration of Mg''_{Ti} ions further increases, thus inhibiting grain growth.

Figure 3 depicts the dielectric temperature spectra of the (0.4−x)BF-xBMT-0.6BT ceramics. The dielectric constant and loss tangent of x = 0.2 ceramics increase with increasing temperature. The reason is that the content of BF is high, and Fe^{3+} is transformed into Fe^{2+}, resulting in a space charge. As the temperature increases, the space charge polarization increases, resulting in an increase in dielectric constant and loss. The relaxor characteristic can be verified by the frequency dispersion in x = 0.25–0.4 samples. This can be ascribed to the obvious difference in ionic valence states between the A- and B-sites in ABO_3-type perovskites, which results in the observed local PNRs [31]. With the increasing BMT, the relaxation degree of the system increases. Comparing the ceramic samples with the grain size, it can be found that the dielectric temperature curve of the small-grain ceramic samples becomes very flat and broadened, and the maximum dielectric constant decreases significantly compared with the

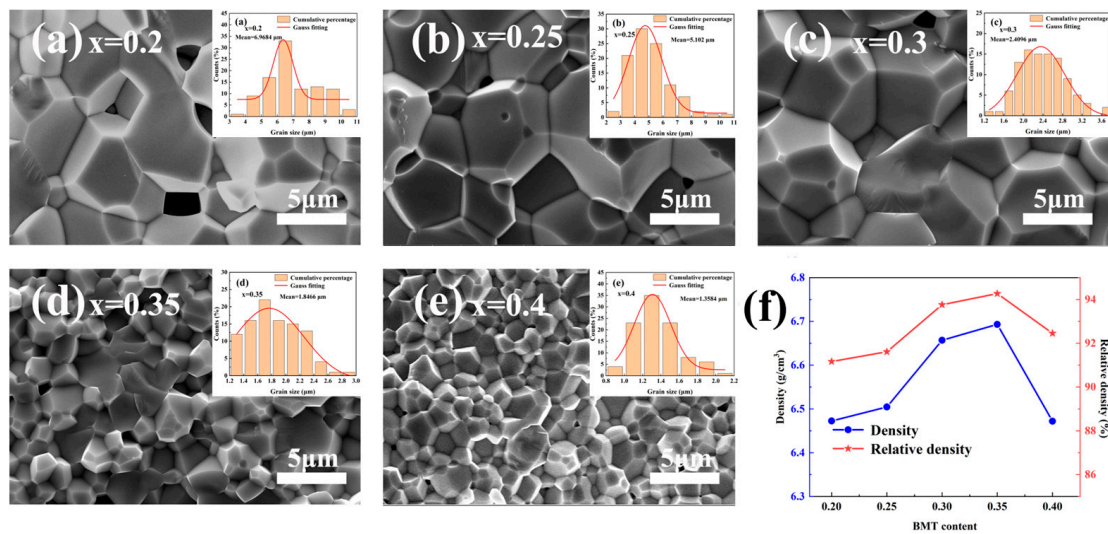large-grain ceramics. The destruction of the ferroelectric long-range order dominates in the rapid decrease in ε_m and widens the ε-T curve of the ceramics.

Figure 2. SEM images of (0.4−x)BF-xBMT-0.6BT bulk ceramics: (**a**) x = 0.2; (**b**) x = 0.25; (**c**) x = 0.3; (**d**) x = 0.35; (**e**) x = 0.4; (**f**) density and relative density.

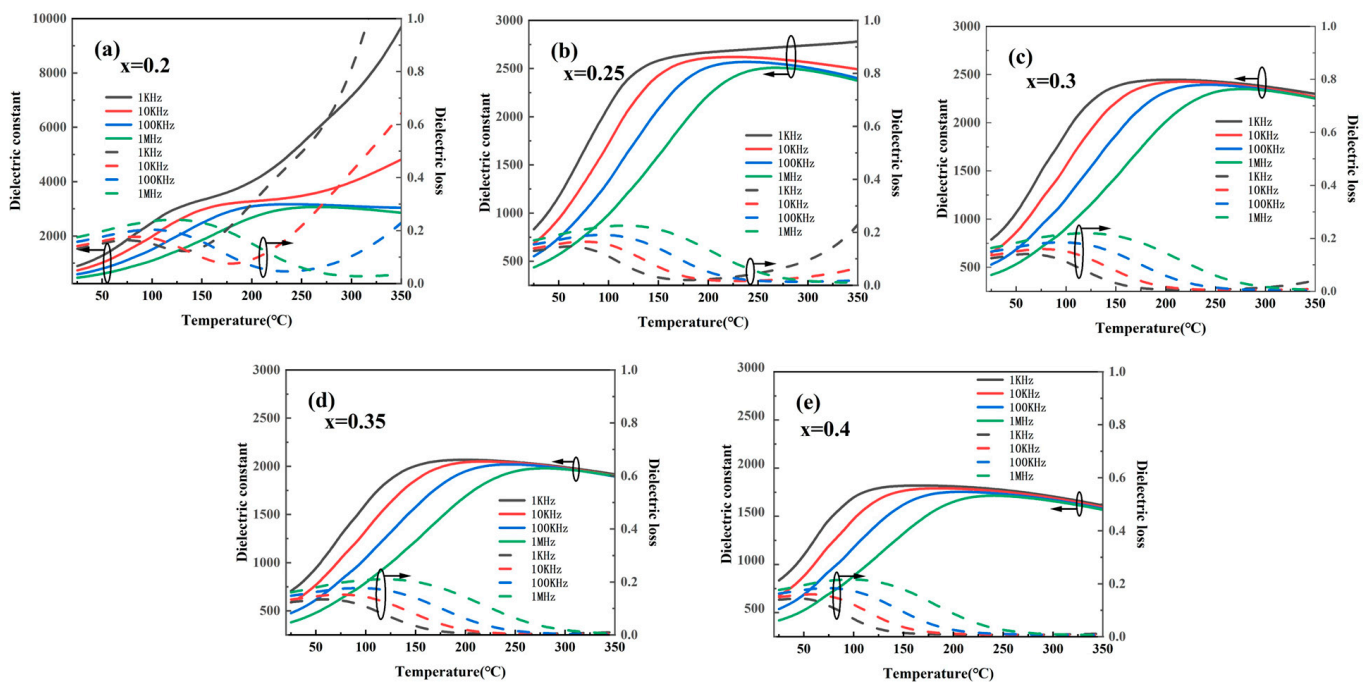**Figure 3.** Dielectric temperature spectra of the (0.4−x)BF-xBMT-0.6BT bulk ceramics with various frequencies: (**a**) x = 0.2; (**b**) x = 0.25; (**c**) x = 0.3; (**d**) x = 0.35; (**e**) x = 0.4.

BDS is one of the most critical physical parameters for pulse power capacitors to optimize the ESPf [32]. The Weibull distribution is a traditional method for assessing the failure reliability of BDS in ceramics, as calculated by the following equations [33–35].

$$X_i = \ln(E_i) \tag{1}$$

$$Y_i = \ln\left[-\ln\left(1 - \frac{i}{n+1}\right)\right] \tag{2}$$

where E_i (kV/cm) represents the experimental breakdown strength of samples, i denotes the numerical order of the samples, and n represents the total number of the tested specimens (n = 8). Between X_i and Y_i, a linear relationship can be established. As denoted by the fitting, the slope can be obtained by β, where β denotes the shape parameter.

As illustrated in Figure 4, β is approximately 10.2, indicating that the breakdown strength is consistent with the Weibull model. The bulk ceramic 0.05BF-0.35BMT-0.6BT has a BDS value of approximately 252 kV/cm.
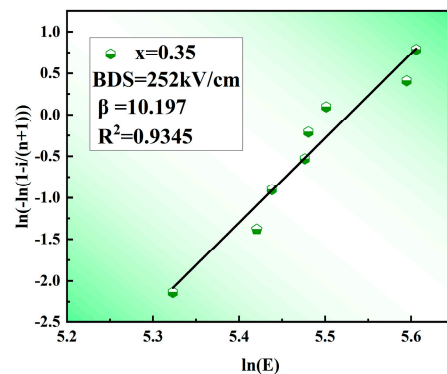

Figure 4. Weibull distribution of the BDS of 0.05BF-0.35BMT-0.6BT ceramics.

The ceramic samples in this experiment are nonlinear dielectric materials. The specific formulas for calculating the energy storage performance of nonlinear dielectrics are as follows [36,37]:

$$W = \int_0^{P_{max}} E\,dP \tag{3}$$

$$W_{rec} = \int_{P_r}^{P_{max}} E\,dP \tag{4}$$

$$\eta = \frac{W_{rec}}{W} \times 100 \tag{5}$$

where W (J/cm^3), W_{rec} (J/cm^3), and η represent the charge energy density, discharge energy density, and efficiency of dielectric ceramics, respectively; P_{max} (μC/cm^2) and P_r (μC/cm^2) refer to the saturated polarization and remnant polarization, respectively; E represents the external electricity. In conclusion, it can be said that high-P_{max} and high-BDS dielectric materials aid in the development of ESPf, whereas low remnant polarization may be advantageous for energy efficiency. Table 1 contains the computed electrical parameters. As depicted in Figure 5, P_{max} decreases from 26.56 μC/cm^2 for x = 0.20 to 19.56 μC/cm^2 for x = 0.40, while P_r decreases from 4.25 μC/cm^2 at x = 0.20 to 1.29 μC/cm^2 at x = 0.40, respectively. However, BMT addition can effectively stop the long-range order of polarization and form polar nano-domains to optimize the BDS of the ceramics. Therefore, in the hysteresis loop shown in Figure 5a, the *P-E* curve becomes increasingly slender as the BMT component increases. In addition, as the BMT component is continuously introduced into the BF-BT ceramics, the BDS of the specimens increases: from 200 kV/cm for x = 0.20 to 270 kV/cm for x = 0.35. The breakdown strength increases because of the BMT; the BF and BT solid solution can reduce the volatilization of Bi, and then reduce the concentration of oxygen vacancies, and the high-valence Ti^{4+} ions replace the Fe^{3+} ions at the B-site, making Fe^{3+} unable to change into Fe^{2+}, reducing the leakage current density. The dielectric constant of the ceramics decreases with the increasing BMT, and the frequency dispersion of the ceramics increases with the broadening and flattening of relaxation peak T_m, which indicates the enhancement of dielectric relaxation. Good ESPf with W = 2.71 J/cm^3 and η = 84.87% at 270 kV/cm can be achieved at x = 0.35. The energy density and unipolar *P-E* loops of the optimum 0.05BF-0.35BMT-0.6BT under E are drawn in Figure 5c,d. The energy density rises significantly until 270 kV/cm, but the η somewhat

declines. The decrease in energy storage efficiency can be attributed to a rise in residual polarization as the applied electric field increases, resulting in increased energy loss.

Table 1. Energy storage properties of (0.4−x)BF-xBMT-0.6BT bulk ceramics at room temperature.

x	P_{max} ($\mu C/cm^2$)	P_r ($\mu C/cm^2$)	BDS (kV/cm)	W (J/cm^3)	W_{rec} (J/cm^3)	η (%)
0.20	26.56	4.25	200	2.64	1.76	66.67
0.25	25.84	3.95	215	2.61	1.83	70.15
0.30	25.27	2.63	225	2.73	2.06	75.46
0.35	22.31	1.42	270	2.71	2.30	84.87
0.40	19.56	1.29	230	2.19	1.70	77.62

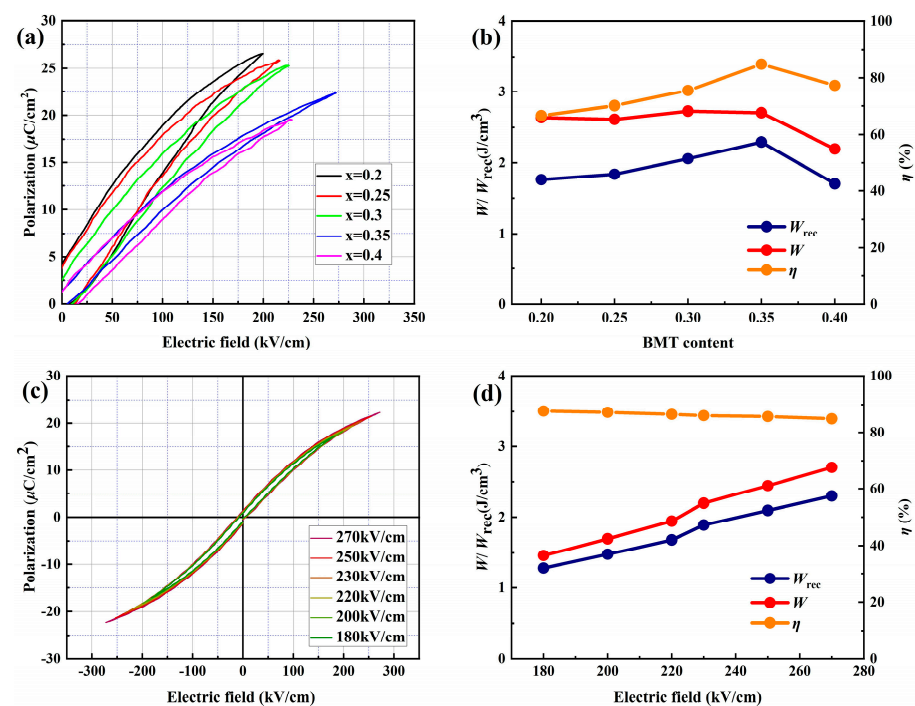**Figure 5.** (**a**) *P-E* loops of (0.4−x)BF-xBMT-0.6BT ceramics under series of electric fields; (**b**) computed ESPf of different compositions; *P-E* curves (**c**) and the computed ESPf (**d**) of 0.05BF-0.35BMT-0.6BT ceramics under different *E* at 10 Hz.

Due to the widespread use of pulsed power technology in aerospace, oil drilling, hybrid vehicles, and other fields, more stringent requirements have been put forward for the working environment of energy storage capacitors. As stated, the dielectric temperature stability and fatigue properties are crucial. The external *E* must be less than 70% of the BDS of the tested ceramics in order to prevent dielectric breakdown. The electric field of 150 kV/cm was selected as the test value in this work.

The *P-E* loops and ESPf of the ceramic 0.05BF-0.35BMT-0.6BT from 20 to 160 °C at 10 Hz and 150 kV/cm are shown in Figure 6a,b. This ceramic displays exceptional temperature stability in ESPf with temperature. Every sample maintains thin loops, and the variation in energy density from 20 to 160 °C is less than 10%, while the efficiency of energy storage remains nearly constant (approximately 80%), which is suitable for high-temperature applications. Additionally, cycling reliability can be used to evaluate the fatigue stability, which is a crucial characteristic in determining the operational lifetimes of dielectric materials.
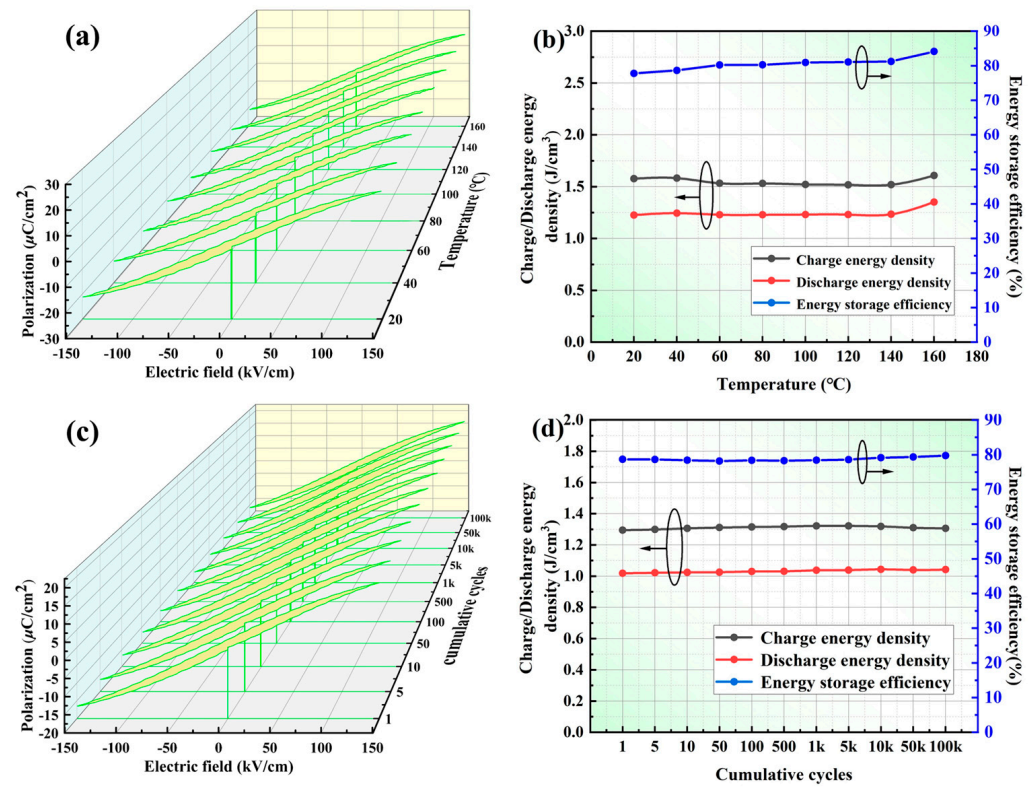
Figure 6. (**a**) Temperature-dependent *P-E* loops, (**b**) temperature-dependent *W*, W_{rec} and efficiency of the 0.05BF-0.35BMT-0.6BT ceramics; (**c**) cyclic *P-E* loops; (**d**) cyclic *W*, W_{rec} and efficiency of the 0.05BF-0.35BMT-0.6BT ceramics.

Figure 6c,d show the *P-E* loops and ESPf of the 0.05BF-0.35BMT-0.6BT ceramics after 10^5 cycles at 10 Hz at 150 kV/cm. As seen in the figure, the ceramic always maintains a slight hysteresis loop after 10^5 cycles, and the remnant polarization does not significantly increase. The *W*, W_{rec}, and η of the ceramics remain almost constant, indicating good cycle stability and a long service life. Bulk ceramic samples of 0.05BF-0.35BMT-0.6BT have outstanding cyclic fatigue and temperature independence, which opens up the possibility of useful applications in diverse situations.

Dielectric capacitors, one of the key elements of pulsed power circuits, typically need to store and release large amounts of energy in a very brief period of time in order to generate a high pulse voltage and large charging current quickly. Discharge time is therefore a crucial factor in energy storage systems and ought to be as low as possible. Here, we used an RC circuit to test the discharge time, speed, and *W* of 0.05BF-0.35BMT-0.6B ceramics. The samples were connected to the load resistance (1000 Ω). Figure 7a,b show the pulsed discharge currents and W of the 0.05BF-0.35BMT-0.6BT ceramics with variable time in different *E*. The current reaches a peak quickly and the duration is very short, indicating that the 0.05BF-0.35BMT-0.6BT ceramics have an extremely quick discharge rate. The formula for calculating the W_{rec} of ceramics is as follows [38].

$$W = \frac{\int I^2(t)R\,dt}{V} \tag{6}$$

where *I* (A) and *t* (s) represent the discharge current and time, while R (Ω) and v denote the total load resistor and the volume of the sample, respectively. Of importance is that *t* can be calculated as $\tau_{0.9}$, denoting the point at which the total energy in the discharge equals 90% of the total energy in storage. As a result, this $\tau_{0.9}$ can always be designed to calculate the discharge rate of the capacitor. The $\tau_{0.9}$ of the sample evaluated with a load resistor of 1000 Ω is 1.3 μs, indicating that it is a promising new type of pulsed power capacitor.
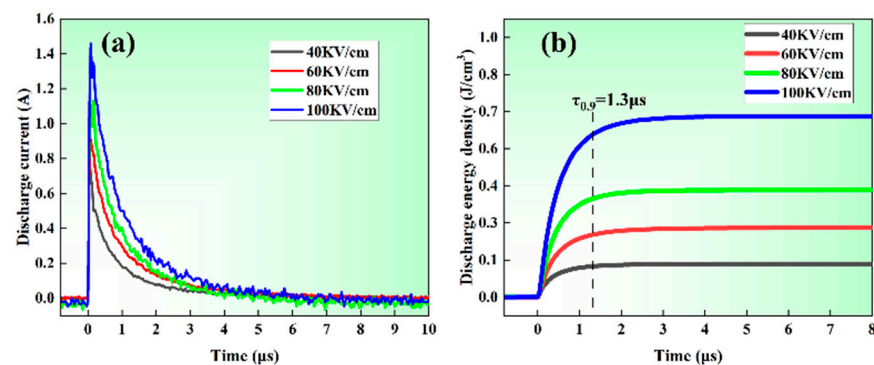
Figure 7. The discharge behavior of the 0.05BF-0.35BMT-0.6BT bulk ceramics at different *E*: (**a**) the pulsed I with discharge time *t* and (**b**) the W_{rec} with discharge time *t*.

Figure 8 presents the comparison of energy storage performance between the 0.05BF-0.35BMT-0.6BT ceramic and other lead-free ceramics reported in recent years [22,39–58]. It can be seen that the 0.05BF-0.35BMT-0.6BT ceramic possesses moderate energy storage performance both in terms of energy storage density and energy storage efficiency.
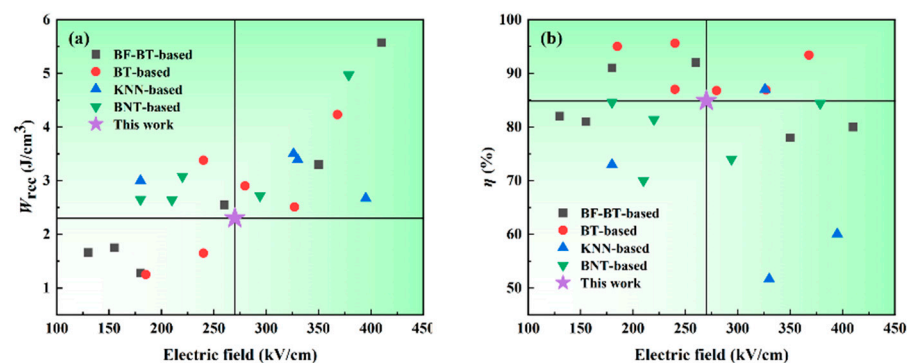

Figure 8. A comparison of (**a**) W_{rec} and (**b**) η as a function of electric field in this study and as reported in other lead-free bulk ceramics (BT-BF-based: [22,39–43]; BaTiO$_3$-based: [44–49]; (K$_{0.5}$Na$_{0.5}$)NbO$_3$-based: [50–54]; Bi$_{0.5}$Na$_{0.5}$TiO$_3$-based: [55–58]).

4. Conclusions

In conclusion, 0.05BF-0.35BMT-0.6BT ceramics were developed with greater energy storage density and effectiveness by compositional modification. With increasing Bi(Mg$_{1/2}$Ti$_{1/2}$)O$_3$ content in (0.4−x)BF-xBMT-0.6BT, this type of ceramic exhibits large relaxation in the dielectric temperature spectra. Furthermore, the addition of an appropriate amount of Bi(Mg$_{1/2}$Ti$_{1/2}$)O$_3$ contributes to the BDS. This could be dependent on the disruption of long-term ordering, which reduces P_r and improves the η. With a W of 2.71 J/cm^3 (W_{rec} = 2.3 J/cm^3) and a η of 84.87% at 270 kV/cm, 0.05BF-0.35BMT-0.6BT ceramics can achieve improved ESPf. The fact that this composition provides great temperature independence up to 160 °C, excellent cycling endurance after 10^5 cycles, and an ultrafast discharge rate of 1.3 µs, respectively, is more significant. As can be inferred, the 0.05BF-0.35BMT-0.6BT eco-friendly ceramics could be a promising competitor for high-power applications such as pulsed power energy storage capacitors, power pulse weapons, and high-speed rail starters.

Data Availability Statement: All data generated or analyzed during this study are included in this article.

Conflicts of Interest: The authors declare no conflict of interest.

References

1. Ma, J.; Zhang, D.; Ying, F.; Li, X.; Li, L.; Guo, S.; Huan, Y.; Zhang, J.; Wang, J.; Zhang, S. Ultrahigh Energy Storage Density and High Efficiency in Lead-Free $(Bi_{0.9}Na_{0.1})(Fe_{0.8}Ti_{0.2})O_3$-Modified NaNbO3 Ceramics via Stabilizing the Antiferroelectric Phase and Enhancing Relaxor Behavior. *ACS Appl. Mater. Inter.* **2022**, *14*, 19704–19713. [CrossRef]
2. Zhao, Y.; Zhang, T.; Sun, L.; Zhao, X.; Tong, L.; Wang, L.; Ding, J.; Ding, Y. Energy storage for black start services: A review. *Int. J. Miner. Metall. Mater.* **2022**, *29*, 691–704. [CrossRef]
3. Ali, A.M.; Hannora, A.E.; El-Falaky, E.; El-Desoky, M.M. Exploring the energy storage density in $60Bi_2O_3$–$10SrO$-$30Fe_2O_3$ lead-free relaxor glass for designing energy storage devices. *J. Non-Cryst. Solids* **2022**, *584*, 121382. [CrossRef]
4. Iba, K. Massive energy storage system for effective usage of renewable energy. *Glob. Energy Interconnect.* **2022**, *5*, 301–308. [CrossRef]
5. Zhang, Y.; Li, S.; He, X.; Zhang, C.; Feng, Y.; Zhang, Y.; Zhang, T.; Wang, X.; Lei, Q.; Chi, Q. Structure, dielectric, ferroelectric, and energy density properties of polyethersulfone-based composite for energy storage application. *J. Mater. Sci. Mater. Electron.* **2022**, *33*, 12884–12899. [CrossRef]
6. Yao, Z.; Song, Z.; Hao, H.; Yu, Z.; Cao, M.; Zhang, S.; Lanagan, M.T.; Liu, H. Homogeneous/inhomogeneous-structured dielectrics and their energy-storage performances. *Adv. Mater.* **2017**, *29*, 1601727. [CrossRef] [PubMed]
7. Yang, L.; Kong, X.; Li, F.; Hao, H.; Cheng, Z.; Liu, H.; Li, J.; Zhang, S. Perovskite lead-free dielectrics for energy storage applications. *Prog. Mater. Sci.* **2019**, *102*, 72–108. [CrossRef]
8. Zhang, Y.; Chi, Q.; Liu, L.; Zhang, C.; Chen, C.; Wang, X.; Lei, Q. Enhanced electric polarization and breakdown strength in the all-organic sandwich-structured poly (vinylidene fluoride)-based dielectric film for high energy density capacitor. *APL Mater.* **2017**, *5*, 76109. [CrossRef]
9. Zhang, T.F.; Tang, X.G.; Liu, Q.X.; Jiang, Y.P.; Huang, X.X.; Zhou, Q.F. Energy-storage properties and high-temperature dielectric relaxation behaviors of relaxor ferroelectric Pb $(Mg_{1/3}Nb_{2/3})O_3$–$PbTiO_3$ ceramics. *J. Phys. D Appl. Phys.* **2016**, *49*, 95302. [CrossRef]
10. Cheng, H.; Ouyang, J.; Zhang, Y.; Ascienzo, D.; Li, Y.; Zhao, Y.; Ren, Y. Demonstration of ultra-high recyclable energy densities in domain-engineered ferroelectric films. *Nat. Commun.* **2017**, *8*, 1999. [CrossRef]
11. Wang, Y.; Shen, Z.; Li, Y.; Wang, Z.; Luo, W.; Hong, Y. Optimization of energy storage density and efficiency in $Ba_xSr_{1-x}TiO_3$ ($x \leq 0.4$) paraelectric ceramics. *Ceram. Int.* **2015**, *41*, 8252–8256. [CrossRef]
12. Yang, L.; Kong, X.; Cheng, Z.; Zhang, S. Ultra-high energy storage performance with mitigated polarization saturation in lead-free relaxors. *J. Mater. Chem. A* **2019**, *7*, 8573–8580. [CrossRef]
13. Shao, T.; Du, H.; Ma, H.; Qu, S.; Wang, J.; Wang, J.; Wei, X.; Xu, Z. Potassium–sodium niobate based lead-free ceramics: Novel electrical energy storage materials. *J. Mater. Chem. A* **2017**, *5*, 554–563. [CrossRef]
14. Yang, Z.; Du, H.; Qu, S.; Hou, Y.; Ma, H.; Wang, J.; Wang, J.; Wei, X.; Xu, Z. Significantly enhanced recoverable energy storage density in potassium–sodium niobate-based lead free ceramics. *J. Mater. Chem. A* **2016**, *4*, 13778–13785. [CrossRef]
15. Liu, N.; Liang, R.; Zhou, Z.; Dong, X. Designing lead-free bismuth ferrite-based ceramics learning from relaxor ferroelectric behavior for simultaneous high energy density and efficiency under low electric field. *J. Mater. Chem. C* **2018**, *6*, 10211–10217. [CrossRef]
16. Yan, F.; Zhou, X.; He, X.; Bai, H.; Wu, S.; Shen, B.; Zhai, J. Superior energy storage properties and excellent stability achieved in environment-friendly ferroelectrics via composition design strategy. *Nano Energy* **2020**, *75*, 105012. [CrossRef]
17. Qi, H.; Zuo, R.; Xie, A.; Tian, A.; Fu, J.; Zhang, Y.; Zhang, S. Ultrahigh energy-storage density in $NaNbO_3$-based lead-free relaxor antiferroelectric ceramics with nanoscale domains. *Adv. Funct. Mater.* **2019**, *29*, 1903877. [CrossRef]
18. Qi, H.; Xie, A.; Tian, A.; Zuo, R. Superior energy-storage capacitors with simultaneously giant energy density and efficiency using nanodomain engineered $BiFeO_3$-$BaTiO_3$-$NaNbO_3$ lead-free bulk ferroelectrics. *Adv. Energy Mater.* **2020**, *10*, 1903338. [CrossRef]
19. Wang, D.; Khesro, A.; Murakami, S.; Feteira, A.; Zhao, Q.; Reaney, I.M. Temperature dependent, large electromechanical strain in Nd-doped $BiFeO_3$-$BaTiO_3$ lead-free ceramics. *J. Eur. Ceram. Soc.* **2017**, *37*, 1857–1860. [CrossRef]
20. Zheng, Q.; Luo, L.; Lam, K.H.; Jiang, N.; Guo, Y.; Lin, D. Enhanced ferroelectricity, piezoelectricity, and ferromagnetism in Nd-modified $BiFeO_3$-$BaTiO_3$ lead-free ceramics. *J. Appl. Phys.* **2014**, *116*, 184101. [CrossRef]
21. Lee, M.H.; Kim, D.J.; Choi, H.I.; Kim, M.; Song, T.K.; Kim, W.; Do, D. Thermal quenching effects on the ferroelectric and piezoelectric properties of $BiFeO_3$–$BaTiO_3$ ceramics. *ACS Appl. Electron. Mater.* **2019**, *1*, 1772–1780. [CrossRef]
22. Zheng, D.; Zuo, R. Enhanced energy storage properties in $La(Mg_{1/2}Ti_{1/2})O_3$-modified $BiFeO_3$-$BaTiO_3$ lead-free relaxor ferroelectric ceramics within a wide temperature range. *J. Eur. Ceram. Soc.* **2017**, *37*, 413–418. [CrossRef]

23. Zheng, D.; Zuo, R.; Zhang, D.; Li, Y. Novel $BiFeO_3$–$BaTiO_3$–$Ba(Mg_{1/3}Nb_{2/3})O_3$ lead-free relaxor ferroelectric ceramics for energy-storage capacitors. *J. Am. Ceram. Soc.* **2015**, *98*, 2692–2695. [CrossRef]

24. Wang, T.; Jin, L.; Tian, Y.; Shu, L.; Hu, Q.; Wei, X. Microstructure and ferroelectric properties of Nb_2O_5-modified $BiFeO_3$-$BaTiO_3$ lead-free ceramics for energy storage. *Mater. Lett.* **2014**, *137*, 79–81. [CrossRef]

25. Zhu, L.; Lei, X.; Zhao, L.; Hussain, M.I.; Zhao, G.; Zhang, B. Phase structure and energy storage performance for $BiFeO_3$–$BaTiO_3$ based lead-free ferroelectric ceramics. *Ceram. Int.* **2019**, *45*, 20266–20275. [CrossRef]

26. Wang, D.; Fan, Z.; Zhou, D.; Khesro, A.; Murakami, S.; Feteira, A.; Zhao, Q.; Tan, X.; Reaney, I.M. Bismuth ferrite-based lead-free ceramics and multilayers with high recoverable energy density. *J. Mater. Chem. A* **2018**, *6*, 4133–4144. [CrossRef]

27. Chen, Z.; Bai, X.; Wang, H.; Du, J.; Bai, W.; Li, L.; Wen, F.; Zheng, P.; Wu, W.; Zheng, L. Achieving high-energy storage performance in $0.67Bi_{1-x}Sm_xFeO_3$-0.33 $BaTiO_3$ lead-free relaxor ferroelectric ceramics. *Ceram. Int.* **2020**, *46*, 11549–11555. [CrossRef]

28. Ubic, R. Revised method for the prediction of lattice constants in cubic and pseudocubic perovskites. *J. Am. Ceram. Soc.* **2007**, *90*, 3326–3330. [CrossRef]

29. Shannon, R.D. Revised effective ionic radii and systematic studies of interatomic distances in halides and chalcogenides. *Acta Crystallogr. Sect. A Cryst. Phys. Diffr. Theor. Gen. Crystallogr.* **1976**, *32*, 751–767. [CrossRef]

30. Chen, X.; Chen, J.; Ma, D.; Fang, L.; Zhou, H. High relative permittivity, low dielectric loss and good thermal stability of $BaTiO_3$-$Bi(Mg_{0.5}Zr_{0.5})O_3$ solid solution. *Ceram. Int.* **2015**, *41*, 2081–2088. [CrossRef]

31. Jo, W.; Schaab, S.; Sapper, E.; Schmitt, L.A.; Kleebe, H.; Bell, A.J.; Rödel, J. On the phase identity and its thermal evolution of lead free $(Bi_{1/2}Na_{1/2})TiO_3$-6mol% $BaTiO_3$. *J. Appl. Phys.* **2011**, *110*, 74106. [CrossRef]

32. Chen, P.; Yang, C.; Cai, J.; Wang, Z.; Zhang, L.; Shi, W.; Jing, J.; Wei, F.; Yan, Y.; Yu, K. Effect of bismuth excess on the energy storage performance of $0.5Na_{0.5}Bi_{0.5}TiO_3$–$0.5SrTiO_3$ ceramics. *Mater. Res. Express* **2019**, *6*, 126306. [CrossRef]

33. Kishimoto, A.; Endo, K.; Motohira, N.; Nakamura, Y.; Yanagida, H.; Miyayama, M. Strength distribution of titania ceramics after high-voltage screening. *J. Mater. Sci.* **1996**, *31*, 3419–3425. [CrossRef]

34. Yang, H.; Yan, F.; Lin, Y.; Wang, T. Enhanced energy storage properties of $Ba_{0.4}Sr_{0.6}TiO_3$ lead-free ceramics with Bi_2O_3-B_2O_3-SiO_2 glass addition. *J. Eur. Ceram. Soc.* **2018**, *38*, 1367–1373. [CrossRef]

35. Huang, Y.; Li, F.; Hao, H.; Xia, F.; Liu, H.; Zhang, S. $(Bi_{0.51}Na_{0.47})TiO_3$ based lead free ceramics with high energy density and efficiency. *J. Mater.* **2019**, *5*, 385–393. [CrossRef]

36. Dang, Z.M.; Yuan, J.K.; Yao, S.H.; Liao, R.J. Flexible nanodielectric materials with high permittivity for power energy storage. *Adv. Mater.* **2013**, *25*, 6334–6365. [CrossRef]

37. Xu, Q.; Liu, H.; Zhang, L.; Xie, J.; Hao, H.; Cao, M.; Yao, Z.; Lanagan, M.T. Structure and electrical properties of lead-free $Bi_{0.5}Na_{0.5}TiO_3$-based ceramics for energy-storage applications. *RSC Adv.* **2016**, *6*, 59280–59291. [CrossRef]

38. Xu, R.; Li, B.; Tian, J.; Xu, Z.; Feng, Y.; Wei, X.; Huang, D.; Yang, L. $Pb_{0.94}La_{0.04}$ [$(Zr_{0.70}Sn_{0.30})_{0.90}$ $Ti_{0.10}$]O_3 antiferroelectric bulk ceramics for pulsed capacitors with high energy and power density. *Appl. Phys. Lett.* **2017**, *110*, 142904. [CrossRef]

39. Tang, M.; Yu, L.; Wang, Y.; Lv, J.; Dong, J.; Guo, B.; Chen, F.; Ai, Q.; Luo, Y.; Li, Q. Dielectric, ferroelectric, and energy storage properties of $Ba(Zn_{1/3}Nb_{2/3})O_3$-modfied $BiFeO_3$–$BaTiO_3$ Pb-Free relaxor ferroelectric ceramics. *Ceram. Int.* **2021**, *47*, 3780–3788. [CrossRef]

40. Wang, D.; Zhu, J.; Liu, Z.; Zhang, A.; Wang, C.; Leung, C.M.; Gao, X.; Lu, X.; Zeng, M. Enhanced energy storage performance in $(1-x)Bi_{0.85}Sm_{0.15}FeO_{3-x}Ca_{0.5}Sr_{0.5}Ti_{0.9}Zr_{0.1}O_3$ relaxor ceramics. *J. Alloys Compd.* **2022**, *903*, 163888. [CrossRef]

41. Zhao, J.; Bao, S.; Tang, L.; Shen, Y.; Su, Z.; Yang, F.; Liu, J.; Pan, Z. Improved energy storage performances of lead-free $BiFeO_3$-based ceramics via doping $Sr_{0.7}La_{0.2}TiO_3$. *J. Alloys Compd.* **2022**, *898*, 162795. [CrossRef]

42. Liu, N.; Liang, R.; Zhao, X.; Xu, C.; Zhou, Z.; Dong, X. Novel bismuth ferrite-based lead-free ceramics with high energy and power density. *J. Am. Ceram. Soc.* **2018**, *101*, 3259–3265. [CrossRef]

43. Yan, F.; Shi, Y.; Zhou, X.; Zhu, K.; Shen, B.; Zhai, J. Optimization of polarization and electric field of bismuth ferrite-based ceramics for capacitor applications. *Chem. Eng. J.* **2021**, *417*, 127945. [CrossRef]

44. Wang, L.; Liu, Q.; Zhou, D. Dielectric and energy storage properties of the $(1-x)BaTiO_3$-$xBi(Li_{1/3}Hf_{2/3})O_3$ ($0.08 \leq \times \leq 0.14$) ceramics. *Mater. Lett.* **2021**, *283*, 128823. [CrossRef]

45. Jiang, X.; Hao, H.; Zhang, S.; Lv, J.; Cao, M.; Yao, Z.; Liu, H. Enhanced energy storage and fast discharge properties of $BaTiO_3$ based ceramics modified by $Bi(Mg_{1/2}Zr_{1/2})O_3$. *J. Eur. Ceram. Soc.* **2019**, *39*, 1103–1109. [CrossRef]

46. Liu, Z.; Li, M.; Tang, Z.; Tang, X. Enhanced energy storage density and efficiency in lead-free $Bi(Mg_{1/2}Hf_{1/2})O_3$-modified $BaTiO_3$ ceramics. *Chem. Eng. J.* **2021**, *418*, 129379. [CrossRef]

47. Lin, Y.; Li, D.; Zhang, M.; Zhan, S.; Yang, Y.; Yang, H.; Yuan, Q. Excellent energy-storage properties achieved in $BaTiO_3$-based lead-free relaxor ferroelectric ceramics via domain engineering on the nanoscale. *ACS Appl. Mater. Inter.* **2019**, *11*, 36824–36830. [CrossRef] [PubMed]

48. Dong, X.; Li, X.; Chen, X.; Wu, J.; Zhou, H. Simultaneous enhancement of polarization and breakdown strength in lead-free $BaTiO_3$-based ceramics. *Chem. Eng. J.* **2021**, *409*, 128231. [CrossRef]

49. Yuan, Q.; Li, G.; Yao, F.; Cheng, S.; Wang, Y.; Ma, R.; Mi, S.; Gu, M.; Wang, K.; Li, J. Simultaneously achieved temperature-insensitive high energy density and efficiency in domain engineered $BaTiO_3$-$Bi(Mg_{0.5}Zr_{0.5})O_3$ lead-free relaxor ferroelectrics. *Nano Energy* **2018**, *52*, 203–210. [CrossRef]

50. Dai, Z.; Li, D.; Zhou, Z.; Zhou, S.; Liu, W.; Liu, J.; Wang, X.; Ren, X. A strategy for high performance of energy storage and transparency in KNN-based ferroelectric ceramics. *Chem. Eng. J.* **2022**, *427*, 131959. [CrossRef]

51. Zhang, M.; Yang, H.; Li, D.; Lin, Y. Excellent energy density and power density achieved in $K_{0.5}Na_{0.5}NbO_3$-based ceramics with high optical transparency. *J. Alloys Compd.* **2020**, *829*, 154565. [CrossRef]

52. Zhang, M.; Yang, H.; Li, D.; Ma, L.; Lin, Y. Giant energy storage efficiency and high recoverable energy storage density achieved in $K_{0.5}Na_{0.5}NbO_3$-$Bi(Zn_{0.5}Zr_{0.5})O_3$ ceramics. *J. Mater. Chem. C* **2020**, *8*, 8777–8785. [CrossRef]

53. Chai, Q.; Yang, D.; Zhao, X.; Chao, X.; Yang, Z. Lead-free (K, Na) NbO_3-based ceramics with high optical transparency and large energy storage ability. *J. Am. Ceram. Soc.* **2018**, *101*, 2321–2329. [CrossRef]

54. Yang, H.; Liu, P.; Yan, F.; Lin, Y.; Wang, T. A novel lead-free ceramic with layered structure for high energy storage applications. *J. Alloys Compd.* **2019**, *773*, 244–249. [CrossRef]

55. Pan, Z.; Hu, D.; Zhang, Y.; Liu, J.; Shen, B.; Zhai, J. Achieving high discharge energy density and efficiency with NBT-based ceramics for application in capacitors. *J. Mater. Chem. C* **2019**, *7*, 4072–4078. [CrossRef]

56. Wu, Y.; Fan, Y.; Liu, N.; Peng, P.; Zhou, M.; Yan, S.; Cao, F.; Dong, X.; Wang, G. Enhanced energy storage properties in sodium bismuth titanate-based ceramics for dielectric capacitor applications. *J. Mater. Chem. C* **2019**, *7*, 6222–6230. [CrossRef]

57. Yang, Y.; Xu, J.; Yang, L.; Zhou, C.; Zhang, H.; Zhang, G.; Wang, H.; Rao, G.; Huo, Z.; Liu, X. Highly enhanced discharged energy density and superior cyclic stability of $Bi_{0.5}Na_{0.5}TiO_3$-based ceramics by introducing $Sr_{0.7}Ca_{0.3}TiO_3$ component. *Mater. Chem. Phys.* **2022**, *276*, 125402. [CrossRef]

58. Shi, P.; Zhu, X.; Lou, X.; Yang, B.; Liu, Q.; Kong, C.; Yang, S.; He, L.; Kang, R.; Zhao, J. Tailoring ferroelectric polarization and relaxation of BNT-based lead-free relaxors for superior energy storage properties. *Chem. Eng. J.* **2022**, *428*, 132612. [CrossRef]